Contents

1 Introduction

2 Plastic Deformation of Silicon Nanowires

The experiments presented so far were conducted at temperatures high enough to ensure that the irradiated material remains crystalline. This ensures that also the density and shape of the nanowires could be preserved. The following chapter discusses the new effect of plastic deformation, which occurs in the room-temperature irradiation of Si-nanowires. Some of the experiments were performed together with Stefan Noack and are published in his Master Thesis [Noa14] and also in reference [JNW$^+$15].

2.1 Experimental observation of plastic deformation

Silicon nanowires where irradiated at room-temperature with high fluences of As^+ and In^+ and/or Ga^+ with the goal of forming Si-$GaAs$ or Si-$InGaAs$ hetero-structures in a further annealing step [PGL$^+$14, Gla15]. To characterize the process, the same individual wires were investigated after each process step, including before and after the irradiation. Two exemplary sets of SEM images of these samples can be seen in figure 2.1. Clearly the nanowires shrank and widened during the irradiation, an effect, that has so far not been reported for irradiation of Si at such low ion energies. This is a plastic deformation caused by the impinging ions, as it is stable even up to high annealing temperatures [PGL$^+$14, Gla15].

To investigate this deformation effect systematically, Si-nanowire arrays similar to the ones used for the sputtering experiment in chapter **??** were irradiated with a set of Ar^+ fluences, rotating the samples under the ion beam. Argon was chosen for the irradiation to avoid any chemical effects, the rotation

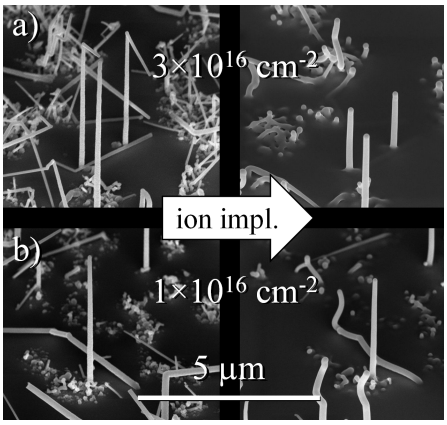

Figure 2.1: SEM images of VLS-grown Si-nanowires before and after the irradiation with $90\,keV\ In^+$ and $120\,keV\ As^+$ at room temperature, while rotating the sample. The shrinking and widening of the wires is clearly visible and larger in the samples irradiated with a high fluence a) of each ion, than in those with a low fluence b).

prevented bending of the nanowires, which would have made the quantification of the deformation difficult. High-resolution SEM images were made after each irradiated fluence to observe and quantify the deformation. Using the algorithm described in chapter **??**, the profiles for the irradiated nanowires were extracted. In figure 2.2 the black, red, green and blue lines show the diameter versus height of a single nanowire before and after irradiation with $100\,keV\ Ar^+$ up to fluences of 1, 3 and $5 \times 10^{16}\,cm^{-2}$ respectively. In this graph, as well as in the inset black profiles, the reduction of the height by $\approx 500\,nm$ and an increase of the diameter, especially at the base, can be clearly seen.

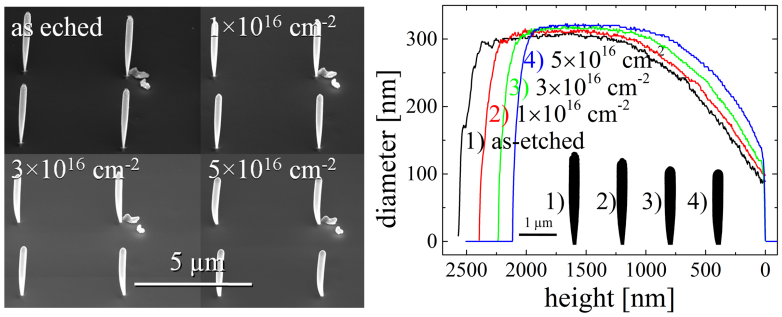

Figure 2.2: Diameter over height of a single Si nanowire irradiated with increasing fluences of $100\,keV\,Ar^+$ ions. The black insets show the profiles of the nanowire after the respective fluences extracted from SEM images. In both illustrations the shrinking and widening of the nanowire is clearly visible.

The plastic deformation does not occur during irradiation of cristalline Si-nanowires at elevated temperatures, as shown in chapter **??**. Only in room-temperature irradiation, where the Si amorphization threshold of $10^{14}\,{}^{ions}/_{cm^2}$ for $100\,keV\ Ar^+$ is very low [PMB04], is the deformation observed. Nanowires first amorphized by ion irradiation and subsequently irradiated at $300°C$ are also deformed. Therefore, it can be concluded, that the plastic deformation under ion irradiation is an attribute of amorphous Si. In crystalline Si irradiated at elevated temperatures the efficient recombination of defects or even recrystallization of disordered sections reimposes the long range order of the crystal lattice on the ion-damaged region, preventing any deformation.

2.2 Quantification of the Deformation

The deformation of the nanowires can be roughly quantified by simply fitting a linear trend to the fluence dependence of the height of the wires. This yields an average of 3% shrinkage per $10^{16}\,{}^{ions}/_{cm^2}$. Due to outliers with larger deformation the values obtained for the 21 nanowires investigated have a large standard deviation of 3% shrinking per $10^{16}\,{}^{ions}/_{cm^2}$. The tendency of the nanowires to bend during the irradiation made the evaluation of more nanowires impossible. However, a more thorough investigation of the deformation is possible by also accounting for the height dependence of the diameter seen in figure 2.2. On average a certain number of atoms are displaced by a certain distance along the height z of the nanowire per ion. Considering only the movement along the height z, a mass-transport rate (MTR) can be calculated according to equation 2.1:

$$\begin{aligned} MTR_{(1\to 2)} &= [{}^1N \cdot {}^1z_c - {}^2z_c \cdot {}^2N - ({}^1N - {}^2N) \cdot {}^2z_c]/N_{ion} \\ &= {}^1N \cdot ({}^1z_c - {}^2z_c)/N_{ion} \end{aligned} \tag{2.1}$$

In equation 2.1 and figure 2.3, ${}^{1/2}z_c$ is the height of the center of mass of the nanowire with the top left index indicating before (^{1}) and after (^{2}) irradiation respectively. The number of atoms at height z_i can be calculated from the local radius r_i. Summing up the height weighted by the number of atoms at that height $z_c \cdot N = \sum_i \pi r_i^2 h \cdot \rho \cdot z_i$ and dividing this by the total number of

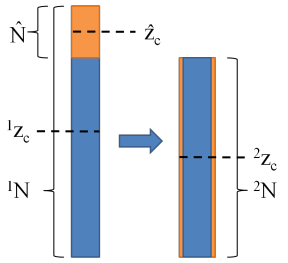

Figure 2.3: Illustration of the mass-transport rate calculation. Displacing ${}^1N$ atoms from their average height ${}^1z_c$ to the average height ${}^2z_c$ requires the same mass-transport, as moving $\hat{N}$ from $\hat{z}_c$ to ${}^2z_c$, taking into account the number of sputtered atoms ${}^1N - {}^2N$.

atoms $N = \sum_i \pi r_i^2 h \cdot \rho$ in the nanowire gives us z_c. The sums are over all slices i of height $h = 1\,pixel = 2.7\,nm$ (typically) each. The number of ions that hit the nanowire during the irradiation of fluence Φ_{12} between making SEM images 1 and 2 is $N_{ion} = \sum_i ({}^1r_i + {}^2r_i) \cdot sin(45°) \cdot h \cdot \Phi_{12}$. The last term in equation 2.1 accounts for the influence of sputtered atoms. Just as in chapter **??** on sputtering, the sputter yield could be calculated by $({}^1N - {}^2N)/N_{ion}$. Figure 2.3 illustrates two interpretations of the MTR calculation. As only the displacement along z is considered, the direct interpretation of equation 2.1 of moving ${}^1N$ atoms from their center of mass ${}^1z_c$ to a new center of mass ${}^2z_c$ is equivalent to moving the atoms which are 'missing' at the top of the nanowire after the irradiation ($\hat{N}$, orange volume in figure 2.3) from their center of mass $\hat{z}$ to ${}^2z_c$, and subtracting the sputtered atoms. This evaluation yields an average mass-transport rate of $1.2 \cdot 10^4\,{}^{atoms \cdot nm}/_{ion}$ with a standard deviation of $7 \cdot 10^3\,{}^{atoms \cdot nm}/_{ion}$. Again the large standard deviation is mainly due to outliers with larger deformation, as can be seen in the histogram of the evaluated mass-trasport rates for a couple of nanowires in figure [**?**].

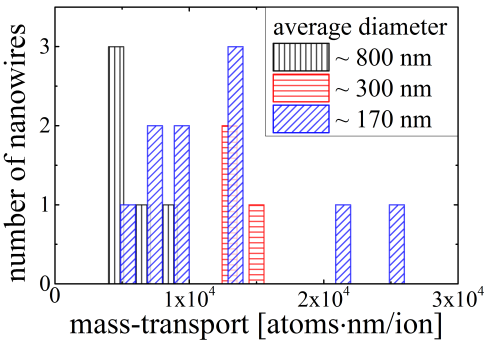

Figure 2.4: Histogram of the results of all mass-transport rates evaluated from the deformation of individual nanowires. Due to the large spread of the data points, no significant correlation between the average diameter nor the ion energy can be shown.

2.3 Knock-on transport of mass

A possible explanation for this observed plastic deformation can be sought in the linear cascade theory, which is applicable for the cascades of $100\,keV\ Ar^+$ in Si: In a collision cascade following an energetic ion impinging a solid, atoms will be preferentially 'knocked-on' along the propagation direction of the impinging ion. This causes an inhomogeneous distribution of interstitials and vacancies and effectively, mass is transported 'downstream' along the ion beam. In an amorphous material it is not clear what constitutes an 'interstitial' or a 'vacancy', but a local excess of vacancies can be understood as a locally decreased density, while an interstitial excess corresponds to an increased density. A local density gradient is not stable, since the density of amorphous Si before and after irradiation is not significantly different [PMB04]. Therefore, the density gradient introduces stress in the material, which can relax by plastic deformation, possibly enabled by a decreased viscosity due to further ion irradiation [SBB97, HCA02, MAAA03, MA03].

As was shown in chapter **??** on sputtering, BCA simulation software can accurately reproduce linear collision cascades. Therefore, a comparison between the experiments and a simulation with *iradina* can evaluate whether the deformation observed in the experiment can be accounted for by knock-on mass transport. Figure 2.5a shows the $600\,nm$ long Si cylinder with a diameter of $200\,nm$ implemented in *iradina* with $2\times2\times2\,nm^3$ voxels in a simulation volume of $204\times204\times600\,nm^3$. The $100\,keV\ Ar^+$ ions impinge at an angle of 45° to the z-axis. They strike the cylinder distributed uniformly along the y-direction at height $z=0$. Figure 2.5d shows the resulting distribution of interstitials on the cross-sectional slice through the middle of the nanowire along the xz plane. This can be seen as an approximation for the distribution of the nuclear energy loss and shows the mean extent of the collision cascade. Figure 2.5e shows the same cross-section after subtracting the number of vacancies produced per ion from the number of interstitials. The excess of vacancies along the impinging plane (blue cone in the cross section) enveloped by two red planes of excess interstitials shows that there is a high probability for the ions to hit a target atom with a large impact parameter. This changes the ions path only little and displaces the target atom in an direction perpendicular to the ion beam. Superimposing many collisions along the y direction

leads to the formation of one vacancy rich and two interstitial rich planes. The xy-plane in 2.5b shows the sum over the height z of the difference between interstitials and vacancies plotted to the same color scale. The illustration is dominated by vacancies at the surface of the cylinder, which are left behind by sputtered atoms.

The height distribution (summing over the radial xy plane) of the interstitials, vacancies and leaving atoms is shown in 2.5c. As expected, the majority of sputtered atoms originate near the impact height. The lines showing the interstitials and vacancies overlap in this illustration. The vacancies subtracted from the sum of interstitials and leaving atoms is plotted along the height in 2.5f. As a displaced atom, leaving behind a vacancy, is either sputtered or becomes an interstitial, the sum over all heights of of this graph is zero. The strong oscillation around $z = 0$ in 2.5f is caused by the previously discussed displacement of target atoms at an angle almost perpendicular to the ion beam for large impact parameters. This oscillation is very sensitive to the voxel-size as in effect the voxel size defines a recombination length and interstitial and vacancy rich regions are mixed in larger voxels. On the other hand, the excess of vacancies near the impact point ($\leq 70\,nm$) and of interstitials further down along the ion's path ($\approx 100\,nm$) is not sensitive to the voxel size. It can be used to quantify the knock-on mass transport by multiplying the plotted values by their height and integrating over all heights. The influence of the short range oscillation immediately around the impact point disappears as here $z \approx 0$ is small. The value obtained from this calculation is $78 \pm 1\,{}^{atoms \cdot nm}/_{ion}$. Clearly this value is to low to account for the large deformation observed in the experiment where a mass-transport rate of $\geq 1 \times 10^4\,{}^{atoms \cdot nm}/_{ion}$ was assessed.

For all simulations a reasonable value for crystalline Si, $15\,eV$ [CW65], was used for the displacement energy, which governs the creation of interstitials and vacancies in the simulation, as discussed in chapter **??**. However, in amorphous materials it is questionable what this value is supposed to mean, as point defects are not well defined. Therefore, simulations where repeated with the displacement energy set to $0\,eV$. As expected, the number of 'vacancies' and 'interstitials' now produced by the simulation increased dramatically. However, the long range difference between 'vacancies' and 'interstitials' seen in figure 2.5f remains unchanged. This is an indication that the knock-on mass

transport is dominated by the rare events where ions hit the target atoms directly, with low impact parameters. In these cases, a large amount of energy is transferred to the displaced atom leading to a long trajectory, preferentially in line with the ion's momentum. On the other hand, atoms displaced with lower energies are much more numerous, but travel much shorter distances and in a randomly orientated direction. This is because most of the low energy displaced atoms are generated at the end of a branch of the collision cascade, the orientation of the branch having previously been randomized by higher energy collisions. The other low energy recoils originate from collisions with a high impact parameter, which leads to a large angle between the incoming particle's and the displaced particle's momentum, as seen near the impact point as a separation of interstitials and vacancies in figure 2.5e and as the short range oscillation in figure 2.5f. These large angle recoils do not contribute significantly to long range mass transport.

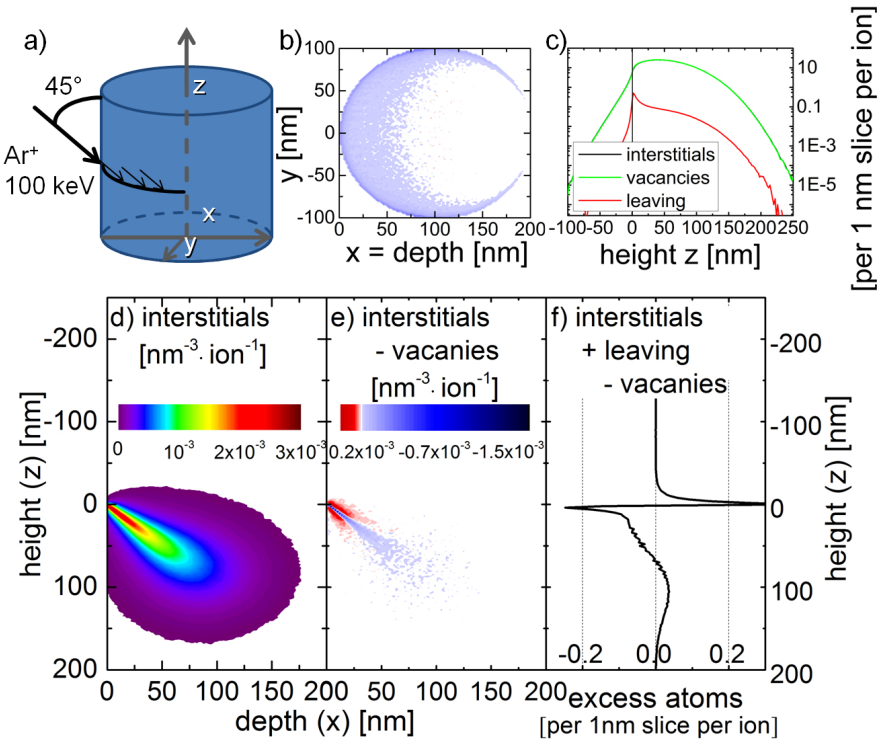

Figure 2.5: a) Illustration of the simulated irradiation geometry. All Ar^+ ions of $100\,keV$ energy hit the nanowire volume at the same height and at an angle of 45° with respect to the nanowire axis z. The created interstitials in the radial cross-section through the middle of the simulated nanowire is shown in d). This distribution is effectively an illustration of the nuclear energy loss. In e) the vacancies are subtracted from the interstitials for the same cross-section. Summing this difference over all heights gives the radial distribution shown in b). The clear dominance of vacancies near the surface is caused by sputtering. The axial profile of the interstitials, vacancies and leaving (sputtered) atoms plotted in c) over the height relative to the impact plane shows that most atoms are sputtered at the impact height. Note that the plots of vacancies and interstitials overlap. The vacancies subtracted from the sum of interstitials and sputtered atoms plotted over the height in f) shows mass transport along the ion's path. Apart from the strong oscillation at the impact height, there is a deficiency of atoms close to the impact height ($\leq 70\,nm$) and an excess centered around $100\,nm$ down from the impact height.

2.4 Irradiation at large angles of incidence

If knock-on mass-transport is not the main contribution to the deformation, the question arises whether the direction of the plastic deformation in the nanowires is related to direction of the ion beam. Will an irradiation from 'below the substrate' towards an unconstrained end of the nanowire also shrink the nanowire, or stretch it out?

Nanowires attached to a substrate are obviously not suited to answering this question, so a method to irradiate nanowires while rotating them at angles greater than 90° to the ion beam was devised. This was achieved by attaching a Si nanowire grown epitaxially on a Si wafer to an Au microwire, which can suspend the nanowire at arbitrary angles in the irradiation chamber. The process is shown in figure 2.6. Platinum deposition by e-beam was used to "glue" the nanowire to the micro-manipulator in the FIB, after which the nanowire was cut from the substrate with the Ga-FIB. Using the Pt-deposition and Ga-FIB again, the nanowire was subsequently attached to the tip of a sharpened Au-microwire, which was previously glued to a piece of wafer for handling and also placed in the FIB chamber. The VLS-grown Si nanowires, similar to those shown in figure 2.1, were used for this experiment as they were readily available in longer lengths ($> 10\mu m$) than the etched nanowires.

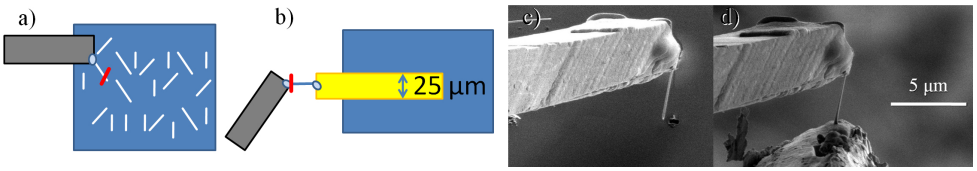

Figure 2.6: Illustration of the nanowire-on-microwire fabrication in a FIB system. The schematic a) and SEM image c) show the nanowire first glued to the micro-manipulator in the FIB by Pt-deposition (light blue ellipse), then cut from the substrate with the Ga-FIB (red line). Images b) and d) Illustrate the subsequent gluing to an Au microwire with Pt-deposition and the final cut with the Ga-FIB to release the nanowire from the micro-manipulator.

The nanowire-on-microwire samples consisted of typically $3-5$ nanowires, each attached to an Au-microwire and arranged in the irradiation chamber on a rotatable stage at an angle of 135° to the ion beam, as shown scematically in figure 2.7a. The alignment of the nanowires to their microwire support was

found to be crucial, as any shadowing of a nanowire from the ion beam an one side would lead to extreme bending of the nanowire. Only a single nanowire was found straight enough to evaluate quantitatively for more than one irradiation step. The SEM images of this nanowire are shown in figure 2.7b-f from a perspective perpendicular to the axis of rotation and rotated by the indicated angle around this axis. The left SEM images show the unirradiated nanowire, while the center and right images were made after the irradiation of $1 \times 10^{16}\, cm^{-2}$ and $3 \times 10^{16}\, cm^{-2}$ $100\, keV$ Ar^{+}, respectively. The unirradiated nanowire is straight and $3.9\, \mu m$ long. The irradiated nanowire shows some bending, so the length had to be determined from a perspective were the curvature of the nanowire is in plane with the image. A fifth order polynomial was fitted to the bent shape and the length of the nanowire was thus determined to be $3.5\, \mu m$ after $1 \times 10^{16}\, cm^{-2}$ (2.7b) and $3.2\, \mu m$ after $3 \times 10^{16}\, cm^{-2}$ (2.7f). The nanowire thus shrank with a similar deformation rate to the previously reported 3% strain per $10^{16}\, {ions}/{cm^2}$, even though the irradiation was directed towards its free end!

2.5 The proposed deformation mechanism

This experiment shows with certainty that the knock-on mass-transport is not the main contributor to the observed deformation, as it would have to be directed along the ion beam. The discussion of a possible model for the deformation will be easier by addressing similar effects and the way that simulation tools were used to understand them. The BCA MC simulation tools available inherently neglect all collective movement of atoms within the target. A field of study that has already faced the limitation of neglecting the local temperature in ion irradiation, is the irradiation with swift, heavy ions. At energies well beyond MeV, the assumption that the dominating effects will be described by binary collisions between the ion and target atoms is false. At high energies and ion masses a significant amount of energy will be transferred form the ion to the electronic system of the target. Through the relaxation mechanisms of the electronic system a part of this energy will be converted to heat in the lattice. Under certain conditions this will form "ion-tracks" in the target. One approach to understand the formation and behavior of ion-tracks is to simulate the longitudinal distribution of the deposited ion en-

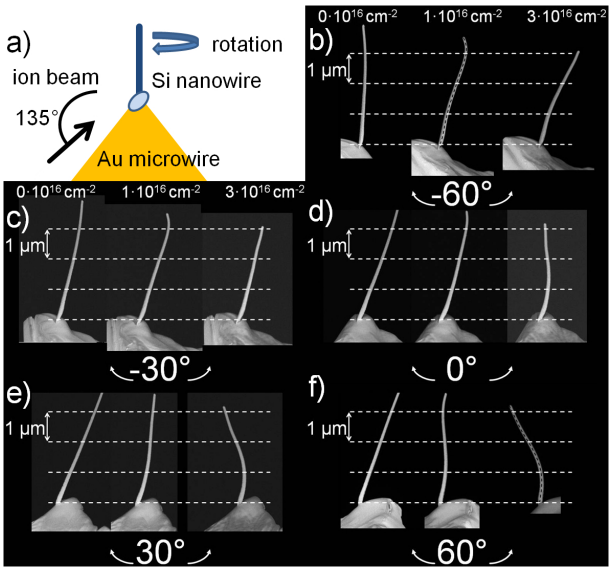

Figure 2.7: a) Illustration of the nanowire-on-microwire irradiation setup. b) - f) SEM images of the same nanowire as-mounted (left SEM images), after irradiation with $1 \times 10^{16}\,cm^{-2}$ (center images), and $3 \times 10^{16}\,cm^{-2}$ (right images) $100\,keV\,Ar^{+}$ ions. The SEM images where taken with the nanowire rotated by the indicated angle from a perspective perpendicular to the angle of rotation. The length of the nanowire after irradiation is determined in b) and f) along the dashed lines.

ergy in the target with BCA tools (typically SRIM) and to evaluate the local temperature in a second step by following the deposited energy according to thermodynamic considerations. A good review of such "thermal spikes" can be found in in reference [WKW04].

Such a thermal spike approach was successful for the description of the plastic deformation by swift heavy ion irradiation according to Trinkaus and Ryazanov [TR95] and in the understanding of material properties governing the direction of the deformation [HKW04, HKW05]. When nanoparticles are deformed [SvBvD$^+$00, SvBvD$^+$01, vDSF$^+$01, DPFB01, DPKB03, DDP$^+$04] an adapted version of the model by Trinkaus can be applied and the effect dubbed "ion hammering" [Kla04]. In short, according to this model the local temperature leads to a transient 'liquid' phase in the cylindrical volume of material around the ion's path. Within the cylindrical geometry, the deformation by thermal expansion is anisotropic and because stresses can relax in the low viscosity volume, this is plastic deformation. This is not observed in materials that remain crystalline during the irradiation, as the long range order of the crystal lattice is reinforced upon the recrystallization during cooling. The problem with directly applying this model to the given situation is that the total energy density in the collision cascade of $100\,keV\,Ar^+$ in Si is a low $\frac{dE}{dx} = 36\,^{eV}/_{nm}$, of which the electronic energy loss is roughly half. Also, the lowest ion energy for which plastic deformation of silica nanoparticles is reported is $300\,keV\,Xe^+$ [DPKB03]. Here, the energy loss is merely $\frac{dE}{dx} = 120\,^{eV}/_{nm}$ with 20 % lost to the electronic system. The threshold for ion tracks, however, is given at $\frac{dE}{dx} \geq 1\,^{keV}/_{nm}$ by Trinkaus et al. [TR95].

The alternative to thermodynamic considerations after a MC BCA simulation are full MD simulations, where the trajectory and interaction of every atom or ion in the simulation volume is followed. This naturally includes all thermal effects, but is limited by computing power to a low number of atoms and thus a severely limited volume of material. Additionally, the accuracy of results depends greatly on finding the interaction potential for all combinations of ions and atoms involved. Here again, as for sputtering, this is true especially for low energy interactions, where these potentials are not available but a topic of research in themselves [Pri12, PGB13]. Investigations of the self-irradiation of $10\,keV\,Si$ and various metals [NGA$^+$98] revealed the formation of nanoscale 'liquid' pockets. The term "liquid" must be used with care as

it refers to a thermodynamical state of matter while the simulation timescale does not allow the assumption of thermodynamic equilibrium. Nevertheless, a sufficiently large number of atoms gain much kinetic energy (say 'are hot') to make the assumption of reduced viscosity and other effects safe. The interesting point of this example is that the energy in the collision cascade was quite low, so that the trajectory of the initiating particle could also have been accurately simulated according to the BCA. A more recent MD investigation by Baumer et al. gets even a step closer to the presented experimental results, in that it predicts plastic deformation in metallic glasses irradiated with high energy neutrons [BD14]. The collision cascades are initiated in $a\text{-}Cu_{50}Nb_{50}$ by assuming primary knock-on atoms of $475\,keV\,Nb$. This atomistic study explicitly shows that plastic deformation due to thermal expansion and stress relaxation can be anisotropic also in collision cascades which do not have the high energy density and symmetry required by the Trinkaus model [TR95]. Somewhat contrary results were obtained by Mayr et al. [MAAA03] where $10\,eV$ to $100\,keV$ recoils of Cu and Ti in $a\text{-}CuTi$ were simulated. That study comes to the conclusion that the viscous flow is dominated by ion induced point defects. It does not propose that knock-on atoms initiate the deformation, but rather, that thermal effects do not provide the main contribution to the reduced viscosity observed during ion irradiation.

The effect of anisotropic deformation within the collision cascade induced by the irradiation of nanowires is shown in figure 2.8a - c. An approximately ellipsoidal volume of the target material is heated by the collision cascade. It expands, becoming more spherical and the anisotropic deformation is retained after cooling. The superimposition of many collision cascades with a similar effect leads to a net contraction along the ion beam $\epsilon_{\parallel} < 0$ and an expansion perpendicular to it $\epsilon_{\perp} > 0$, as shown in 2.8b. To maintain constant density $-2 \cdot \epsilon_{\perp} = \epsilon_{\parallel}$. The rotational average of this deformation around the z-axis, as illustrated in 2.8c, works out to be a contraction along the z-axis $\epsilon_{zz} = {}^1\!/_2\epsilon_{\parallel}$ and a corresponding expansion in the xy-plane for an angle of $\pm\,45°$ between the ion beam and the z-axis. The z-axis represents the nanowire axis, while the xy-plane is parallel to the nanowire diameter. Thus, the deformation rate of $d\epsilon_{zz}/d\Phi = 3\%$ strain per $10^{16}\,{}^{ions}\!/_{cm^2}$ extracted from a linear fit to the reduction of the nanowire height can be transformed into a strain rate parallel to the ion beam of $d\epsilon_{\parallel}/d\Phi = 6\%$ strain per $10^{16}\,{}^{ions}\!/_{cm^2}$, or $6 \cdot 10^{-18}\,{}^{cm^2}\!/_{ion}$.

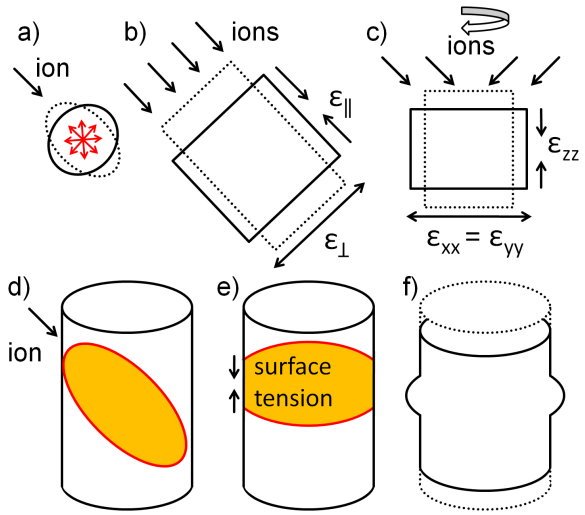

Figure 2.8: a) - c) Illustration of a deformation model analogous to ion hammering. a) The collision cascade from a single impinging ion heats an approximately ellipsoidal volume of the target material. The internal pressure will lead to an expansion towards a more spherical shape, which is retained upon cooling. b) The net effect of many ions is thus a contraction parallel to and an expansion perpendicular to the ion beam. For no change in density $\epsilon_{\parallel} = -2\epsilon_{\perp}$ has to hold. c) Under rotational symmetry this deformation translates to a contraction in the rotational axis z and an expansion in the perpendicular $x - y$ plane with $\epsilon_{zz} = -2\epsilon_{xx} = -\epsilon_{\perp}$. In d) - f) the alternative, surface tension driven deformation is illustrated. The collision-heated volume of target material shown in d). A significant slice of the nanowire shown in e) thus has a reduced viscosity. The surface energy is reduced by an increase in the local diameter of the nanowire, leading to a shortened and thickened nanowire segment shown in f).

This is much less than the values for the studies at higher energies reported in literature. In reference [DPKB03] a strain rate of $10^{-16}\,{}^{cm^2}/_{ion}$ were reported for $300\,keV\ Xe$ in silica nanoparticles and ref. [BD14] even arrives at $10^{-15}\,{}^{cm^2}/_{ion}$ with MD calculations in bulk. There are unfortunately no studies published on straining bulk silicon at these low ion energies, even though bending of thinned Si-wafers similar to [Vol91, MKKP08] would be measurable with the here reported straining rate of 6% strain per $10^{16}\,{}^{ions}/_{cm^2}$ in a layer of $\approx 300\,nm$.

The quantitative discrepancy between the deformation observed in the experiments presented here and published studies may be attributed to the lower ion energy and one may gain confidence in this model due to the qualitative similarity to the MD simulations by Baumer et al. [BD14] also showing deformation anisotropy at relatively low ion energies. However, a further, major difference between the MD simulation and the experiments presented here is the fact that in the presented experiments the collision cascade is not in bulk, but in a nanostructure, were there is not much material around and it is not distributed around the cascade isotropically. If the ellipsoidal volume intersects the nanowire surface, the pressure from the thermal expansion will vent outward removing the force needed to drive the deformation. An more favorable model illustrates that the strong influence of the surface expected in nanowires can also lead to the observed plastic deformation. In figure 2.8d the relation between the nanowire and collision cascade is shown. As there is not much material around, the temperature in a sizable slice of the nanowire will remain elevated for some time [Bor12, GHB$^+$13, ABU15, JHMR15]. In addition the ion irradiation itself will reduce the viscosity [SBB97, HCA02, MAAA03], allowing the surface tension to deform the nanowire by increasing the radius locally. The local increase in diameter reduces the total surface area and thus the surface energy. The nanowire subsequently becomes shorter and wider as shown in figure 2.8f. Further evidence for the surface tension driven plastic deformation can be found in the SEM images in figures 2.1 and 2.2a. The nanowires look smooth and 'molten' after the irradiation, which may be an indication that they underwent a temporary, local phase of low viscosity.

Apart from the bulk deformation experiment already suggested, a further experiment, which could distinguish which of the two models applies, is the irradiation of the nanowires at 90° between the nanowire axis and the ion

beam. In this irradiation geometry, if the first model similar to ion hammering applies the irradiation should produce slowly elongating wires with a reduced radius, as the positive $\epsilon_\perp$ is now parallel to the nanowire axis. On the other hand, if the surface tension driven model is applicable the nanowires will shrink regardless of the irradiation angle. Naturally, a similar nanowire-on-microwire setup to the one for irradiation at 135° could be used to irradiate at 90°. It turns out however, that the irradiation at 90° is extremely prone to bending the nanowires. The bending can be attributed to the Pt deposited used to attach the Si nanowire onto the Au microwire in the FIB. This deposition is concentrated at the base and on one side of the nanowire and thus suppresses the rotational symmetry of the deformation, leading to bending. In the irradiation at 135° the base of the nanowire, where the Pt is deposited, is shadowed from the ion beam by the microwire so that the nanowires are less likely to bend in this configuration. Due to the bending, the angle between the nanowire and the ion beam varied during a rotation cycle, so that a conclusive discrimination between the models can unfortunately not be made.

Summary

Silicon nanowires show plastic deformation when irradiated with $100\,keV\ Ar^+$ ions at room-temperature. Comparison with simulations as well as an explicit experiment both show that the deformation is not mediated by point contacts and not directed along the ion beam. The nanowires shrink at a rate of very roughly 3% per $10^{16}\,{}^{ions}/_{cm^2}$ with no indication of saturation. Due to bending of the nanowires it was not possible to investigate enough nanowires to determine a possible diameter dependence of the plastic deformation. The most likely model for the plastic deformation is driven by surface tension on a low-viscous, small volume of the nanowire near the ion impact point.

3 Conclusions and Outlook

The first conclusion, although it is actually almost a premise to this dissertation, is that sputtering is indeed an important effect that needs considering in high-fluence irradiation. This is especially true in the case of nanostructures where sputter yields can be greatly enhanced, as was shown this dissertation for the example of Si-nanowires. These results show that a good qualitative estimation, or intuition, of how any given nanostructure will be sputtered can be obtained using the Sigmund model for sputtering. The relative size of the overlap of the ions' nuclear energy loss and the surface of the target, even if it is nanostructured, is a reasonable estimation for the relative sputter yield. Thus, a feeling for which part of a complicated nanostructure will be most affected by sputtering during the irradiation with ions of a certain species and energy can be gained. For a specific nanoscale geometry the MC BCA simulation program *iradina* [BR11] can be used to make a more detailed analysis. The diameter dependence of sputter yield simulated with *iradina* is qualitatively reproduced by the experiments performed in this thesis.

The quantitative values of sputtering are, in general, not accessible through the naive use of MC BCA simulations. However, very good agreement can be found for certain material and ion combinations [Bie87, HZM14], so the situation is not at all hopeless. The main difficulty is to find correct low energy interaction potential for the colliding atoms and ions for the given situation. As the secondary ion mass spectrometry (SIMS) technique is highly reliant on sputter yields and MD simulations also require the correct interaction potential at low particle energies, there is some interest in solving this problem. As sputtering is dominated by low energy collisions, it is very sensitive to the interaction potential precisely at the energy range where it is not easily accessible to other experiments. Therefore, experiments on sputtering of defined nanostructures, such as the ones performed on nanowires within this thesis, may be a useful approach to test theoretical predictions based on different

interaction potentials. Such experiments should be combined and compared with ion impact-angle dependent measurements of the sputtering [HZM14] and the angle resolved emission of the sputtered atoms [WM08, VWMS08]. This approach will not produce the correct interaction potential, however, it can be used to test results from simulations with different potentials to determine which describes the inter-atomic interaction best.

The main goal of ion irradiation is typically not sputtering, but the incorporation of dopants in the target. For nanostructured targets, care has to be taken to avoid an inhomogeneous irradiation and doping profile due to shadowing of the ion beam. This was illustrated with the nano-XRF investigation of Mn-doped ZnO nanowires. This investigation shows that the BC MCA simulation is adequate for the prediction of the doping concentration for low ion fluences in nanowires. The limit of this applicability is given by the point where around 20% of the material affected by the ion beam is sputtered, which in nanostructures is typically 20% of the whole nanostructures' volume. Similar approximations can be made in bulk [ME84, And86, MEB88, SO93, ZS95], even if the given references don't explicitly state a limiting fluence or sputtered depth. For irradiations with higher fluences, dynamic simulations are needed to predict the correct dopant concentration and profile. For nanostructures this ion fluence can be much lower than in bulk as there is less material to be sputtered and sputtering is enhanced. For high fluence irradiations, where more than 20% of the material is expected to be sputtered, dynamic simulations are recommended. Software, which can dynamically change the structure and composition of the ion irradiated, nanostructured target, has been revealed recently in reference [Mö14]. A comparison of the experimental results presented in this thesis with the results from such a simulation is a logical next step.

Down these lines, the application of the nano-XRF quantification technique to ion irradiated nanostructures can produce further interesting results. As nano-XRF is highly sensitive to elemental concentrations, it can widen the scope of the proposed studies into sputtering by investigating compositional changes ion irradiated nanostructures of compound materials. In compound materials preferential sputtering of one of the materials' components may become relevant even before a high dopant concentration has been reached. The interplay of nano-structuring, compositional changes and pref-

erential sputtering could thus be investigated for a vast array of materials, by no means limited to semiconductors. Comparison to simulation results would further the understanding of the parameters influencing the preferential sputtering, which has practical meaning in secondary ion mass spectroscopy (SIMS), but also in the development of materials for fusion reactor components [Kel78, Rot90, KOW11]. Using nanowires for such an experiment has the advantage that samples with multiple diameters can be fabricated in parallel and thus a larger parameter space becomes accessible to simultaneous investigation.

The sputtering of nanostructures is enhanced relative to bulk not only because of the high surface to volume ratio, but also by thermal effects. These can be very pronounced if the energy deposited by the impinging ion is confined to a small volume [GHB$^+$13, IKN$^+$14, NSUM14, ABU15, UBNM15]. This can lead to explosive ejection of large clusters of $1000s$ of atoms. Such extreme thermal sputtering effects are not observed in the experiments presented in this thesis; firstly, because the nanowires are relatively large compared to the ion energy deposited in them, leading, on average, to only little energy deposited per atom; secondly, the ion mass and target atom mass are both relatively low, leading to a low stopping power and a low density of the energy deposition. The simulation of sputtering with the BCA and the Sigmund theory would break down in experiments where this is not the case. Nevertheless, the maximum sputter yield observed at lower nanowire diameters in the experiment than in the simulation. This could be caused by increased sputtering due to larger thermal effects in thinner nanowires than in thicker ones.

Silicon nanowires show plastic deformation when irradiated with medium weight Ar^+ ions at room-temperature and energies of $100\,keV$. It could be shown that this deformation is not mediated by point defects and is not directed along the ion beam. Therefore, a surface tension driven model, which relies on a locally reduced viscosity, is presented. Where the lower threshold for the deformation is and whether there is an upper threshold energy above which the deformation ceases is not clear. It is clear, however, that the observed deformation is not in line with the ion track induced plastic deformation proposed by Trinkaus et al. [TR95], as the energy loss of the ion is too low and the locally increased pressure required by this model is not likely to

be confined in the limited volume of a nanowire. The deformation is observed in amorphous Si-nanowires, but not in crystalline Si, both irradiated at elevated temperatures. In the crystalline case, the efficient recrystallization of the ion damaged nanowire volume recreates the long range order of the crystal lattice, while the amorphous material is free to remain deformed.

The plastic deformation of Si, highly localized at the point of the ions impact, has great potential for nanostructuring applications. It may be relevant to the formation of nanopores [GTC$^+$10] and certainly to the bending and manipulation of nanowires [CFL$^+$13] and freestanding films [KCA$^+$06]. It could be possible to go as far as building Si nano-origami [CCJ$^+$13] with suitable templates. This may be a versatile tool in the growing field of Si MEMS devices. Furthermore it may have to be considered in the formulation of a new mechanism for the formation of ripples on ion irradiated Si surfaces. The dated model by Bradley and Harper [BH88] considers only curvature and angle dependent sputtering as a roughening mechanism and is contested by models including ion induced strain and mass-transport [Nor12, KRG14]. The latter shows some similarity with the results presented here, indicating that an atomistic investigation may be necessary to resolve this issue.

All three chapters of this thesis have compared MC BCA simulations performed with *iradina* to experimental results on nanowires irradiated with high fluences. One limit to the applicability of the BCA is found were thermal effects have to be considered. This is not quite the case for the presented diameter-dependent sputter yields, where the simulation overlaps qualitatively with the experimental results. Only a slight shift in the diameter of maximum sputtering may indicate an influence of local, ion-induced heating. However, the plastic deformation found in amorphous Si-nanowires can not be explained with this simulation technique. Furthermore, the accuracy of the prediction of the doping concentration in nanostructures determined with *iradina* simulations is satisfactory, but limited to low ion fluences. When the desired doping concentration is high and high ion fluences have to be implanted, dynamic simulations become neccessary. A rule of thumb lower limit to what constitutes a 'high' fluence is given by the fluence at which 20% of the volume effected by the ion beam is sputtered.

Bibliography

[ABU15] Christian Anders, Eduardo M. Bringa, and Herbert M. Urbassek. Sputtering of a metal nanofoam by Au ions. *Nuclear Instruments and Methods in Physics Research Section B: Beam Interactions with Materials and Atoms*, 342:234–239, January 2015. 00000.

[And86] Hans Henrik Andersen. Computer simulations of atomic collisions in solids with special emphasis on sputtering. *Nuclear Instruments and Methods in Physics Research Section B: Beam Interactions with Materials and Atoms*, 18(1-6):321–343, January 1986.

[BD14] Richard E. Baumer and Michael J. Demkowicz. Prediction of Spontaneous Plastic Deformation of Irradiated Metallic Glasses due to Thermal Spike-Induced Plasticity. *Materials Research Letters*, 2(4):221–226, October 2014.

[BH88] R. Mark Bradley and James M. E. Harper. Theory of ripple topography induced by ion bombardment. *Journal of Vacuum Science & Technology A*, 6(4):2390–2395, July 1988.

[Bie87] J. P. Biersack. Computer simulations of sputtering. *Nuclear Instruments and Methods in Physics Research Section B: Beam Interactions with Materials and Atoms*, 27(1):21–36, June 1987.

[Bor12] Christian Borschel. *Ion-Solid Interaction in Semiconductor Nanowires*. PhD thesis, University Jena, Jena, 2012.

[BR11] C. Borschel and C. Ronning. Ion beam irradiation of nanostructures – A 3d Monte Carlo simulation code. *Nuclear Instruments and Methods in Physics Research Section B: Beam Inter-*

actions with Materials and Atoms, 269(19):2133–2138, October 2011.

[CCJ+13] Khattiya Chalapat, Nikolai Chekurov, Hua Jiang, Jian Li, Babak Parviz, and G. S. Paraoanu. Self-Organized Origami Structures via Ion-Induced Plastic Strain. *Advanced Materials*, 25(1):91–95, January 2013.

[CFL+13] Ajuan Cui, J. C. Fenton, Wuxia Li, Tiehan H. Shen, Zhe Liu, Qiang Luo, and Changzhi Gu. Ion-beam-induced bending of free-standing amorphous nanowires: The importance of the substrate material and charging. *Applied Physics Letters*, 102(21):213112, May 2013.

[CW65] J. W. Corbett and G. D. Watkins. Production of Divacancies and Vacancies by Electron Irradiation of Silicon. *Physical Review*, 138(2A):A555–A560, April 1965.

[DDP+04] T. van Dillen, M. J. A. de Dood, J. J. Penninkhof, A. Polman, S. Roorda, and A. M. Vredenberg. Ion beam-induced anisotropic plastic deformation of silicon microstructures. *Applied Physics Letters*, 84(18):3591–3593, May 2004.

[DPFB01] T. van Dillen, A. Polman, W. Fukarek, and A. van Blaaderen. Energy-dependent anisotropic deformation of colloidal silica particles under MeV Au irradiation. *Applied Physics Letters*, 78(7):910–912, February 2001.

[DPKB03] T. van Dillen, A. Polman, C. M. van Kats, and A. van Blaaderen. Ion beam-induced anisotropic plastic deformation at 300 keV. *Applied Physics Letters*, 83(21):4315–4317, November 2003.

[GHB+13] G. Greaves, J. A. Hinks, P. Busby, N. J. Mellors, A. Ilinov, A. Kuronen, K. Nordlund, and S. E. Donnelly. Enhanced Sputtering Yields from Single-Ion Impacts on Gold Nanorods. *Physical Review Letters*, 111(6):065504, August 2013. 00004.

[Gla15] Markus Glaser. *Personal communication, Thesis in writing.* PhD thesis, TU Wien, Wien, 2015.

[GTC+10] H. Bola George, Yuye Tang, Xi Chen, Jiali Li, John W. Hutchinson, Jene A. Golovchenko, and Michael J. Aziz. Nanopore fabrication in amorphous Si: Viscous flow model and comparison to experiment. *Journal of Applied Physics*, 108(1):014310, July 2010.

[HCA02] Xiaoyuan Hu, David G. Cahill, and Robert S. Averback. Burrowing of Pt nanoparticles into SiO2 during ion-beam irradiation. *Journal of Applied Physics*, 92(7):3995–4000, October 2002.

[HKW04] A Hedler, Siegfried Ludwig Klaumünzer, and Werner Wesch. Amorphous silicon exhibits a glass transition. *Nature Materials*, 3(11):804–809, November 2004.

[HKW05] A. Hedler, S. Klaumünzer, and W. Wesch. Boundary effects on the plastic flow of amorphous layers during high-energy heavy-ion irradiation. *Physical Review B*, 72(5):054108, August 2005.

[HZM14] H. Hofsäss, K. Zhang, and A. Mutzke. Simulation of ion beam sputtering with SDTrimSP, TRIDYN and SRIM. *Applied Surface Science*, 310:134–141, August 2014.

[IKN+14] A. Ilinov, A. Kuronen, K. Nordlund, G. Greaves, J. A. Hinks, P. Busby, N. J. Mellors, and S. E. Donnelly. Sputtering yields exceeding 1000 by 80 keV Xe irradiation of Au nanorods. *Nuclear Instruments and Methods in Physics Research Section B: Beam Interactions with Materials and Atoms*, 341:17–21, December 2014.

[JHMR15] Andreas Johannes, Henry Holland-Moritz, and Carsten Ronning. Ion beam irradiation of nanostructures: sputtering, dopant incorporation, and dynamic annealing. *Semiconductor Science and Technology*, 30(3):033001, March 2015.

[JNW+15] Andreas Johannes, Stefan Noack, Werner Wesch, Markus Glaser, Alois Lugstein, and Carsten Ronning. Anomalous Plastic Deformation and Sputtering of Ion Irradiated Silicon Nanowires. *Nano Letters*, May 2015.

[KCA+06] Y.-R. Kim, P. Chen, M. J. Aziz, D. Branton, and J. J. Vlassak. Focused ion beam induced deflections of freestanding thin films. *Journal of Applied Physics*, 100(10):104322, November 2006.

[Kel78] Roger Kelly. An attempt to understand preferential sputtering. *Nuclear Instruments and Methods*, 149(1–3):553–558, March 1978.

[Kla04] S. Klaumünzer. Ion hammering of silica colloids. *Nuclear Instruments and Methods in Physics Research Section B: Beam Interactions with Materials and Atoms*, 215(3–4):345–352, February 2004.

[KOW11] T. Kenmotsu, T. Ono, and M. Wada. Effect of deuterium retention upon sputtering yield of tungsten by deuterons. *Journal of Nuclear Materials*, 415(1, Supplement):S108–S111, August 2011.

[KRG14] Detlef Kramczynski, Bernhard Reuscher, and Hubert Gnaser. Wavelength-dependent ripple propagation on ion-irradiated prepatterned surfaces driven by viscous flow corroborates two-field continuum model. *Physical Review B*, 89(20):205422, May 2014.

[Mö14] Wolfhard Möller. TRI3dyn – Collisional computer simulation of the dynamic evolution of 3-dimensional nanostructures under ion irradiation. *Nuclear Instruments and Methods in Physics Research Section B: Beam Interactions with Materials and Atoms*, 322:23–33, March 2014. 00001.

[MA03] S. G. Mayr and R. S. Averback. Effect of ion bombardment on stress in thin metal films. *Physical Review B*, 68(21):214105, December 2003.

[MAAA03] S. G. Mayr, Y. Ashkenazy, K. Albe, and R. S. Averback. Mechanisms of Radiation-Induced Viscous Flow: Role of Point Defects. *Physical Review Letters*, 90(5):055505, February 2003.

[ME84] W. Möller and W. Eckstein. Tridyn — A TRIM simulation code including dynamic composition changes. *Nuclear Instruments*

and Methods in Physics Research Section B: Beam Interactions with Materials and Atoms, 2(1–3):814–818, March 1984.

[MEB88] W. Möller, W. Eckstein, and J. P. Biersack. Tridyn-binary collision simulation of atomic collisions and dynamic composition changes in solids. *Computer Physics Communications*, 51(3):355–368, November 1988. 00441.

[MKKP08] S. Massl, H. Köstenbauer, J. Keckes, and R. Pippan. Stress measurement in thin films with the ion beam layer removal method: Influence of experimental errors and parameters. *Thin Solid Films*, 516(23):8655–8662, October 2008.

[NGA+98] K. Nordlund, M. Ghaly, R. S. Averback, M. Caturla, T. Diaz de la Rubia, and J. Tarus. Defect production in collision cascades in elemental semiconductors and fcc metals. *Physical Review B*, 57(13):7556–7570, April 1998.

[Noa14] Stefan Noack. *Sputter Effects of Silicon Nanowires under Ion Bombardment*. University Jena, Master Thesis, 2014.

[Nor12] Scott Norris. Stress-induced patterns in ion-irradiated silicon: Model based on anisotropic plastic flow. *Physical Review B*, 86(23):235405, December 2012.

[NSUM14] Maureen L. Nietiadi, Luis Sandoval, Herbert M. Urbassek, and Wolfhard Möller. Sputtering of Si nanospheres. *Physical Review B*, 90(4):045417, July 2014.

[PGB13] D. Primetzhofer, D. Goebl, and P. Bauer. Local vs. non-local energy loss of low energy ions: Influence of charge exchange processes in close collisions. *Nuclear Instruments and Methods in Physics Research Section B: Beam Interactions with Materials and Atoms*, 317, Part A:8–12, December 2013.

[PGL+14] Slawomir Prucnal, Markus Glaser, Alois Lugstein, Emmerich Bertagnolli, Michael Stoeger-Pollach, Shengqiang Zhou, Manfred Helm, Denis Reichel, Lars Rebohle, Marcin Turek, Jerzy Zuk, and Wolfgang Skorupa. III-V semiconductor

nanocrystal formation in silicon nanowires via liquid-phase epitaxy. *Nano Research*, 7(12):1769–1776, December 2014. WOS:000346641400006.

[PMB04] Lourdes Pelaz, Luis A. Marqués, and Juan Barbolla. Ion-beam-induced amorphization and recrystallization in silicon. *Journal of Applied Physics*, 96(11):5947–5976, December 2004.

[Pri12] D. Primetzhofer. Inelastic energy loss of medium energy H and He ions in Au and Pt: Deviations from velocity proportionality. *Physical Review B*, 86(9):094102, September 2012.

[Rot90] J. Roth. Sputtering of Limiter and Divertor Materials. *Journal of Nuclear Materials*, 176:132–141, December 1990. WOS:A1990FC48200014.

[SBB97] E. Snoeks, K. S. Boutros, and J. Barone. Stress relaxation in tungsten films by ion irradiation. *Applied Physics Letters*, 71(2):267–269, July 1997.

[SO93] Peter Sigmund and Antonino Oliva. Alloy sputtering at high fluence: preferential sputtering and competing effects. *Nuclear Instruments and Methods in Physics Research Section B: Beam Interactions with Materials and Atoms*, 82(2):269–282, July 1993.

[SvBvD+00] E. Snoeks, A. van Blaaderen, T. van Dillen, C. M. van Kats, M. L. Brongersma, and A. Polman. Colloidal Ellipsoids with Continuously Variable Shape. *Advanced Materials*, 12(20):1511–1514, October 2000.

[SvBvD+01] E Snoeks, A van Blaaderen, T van Dillen, C. M van Kats, K Velikov, M. L Brongersma, and A Polman. Colloidal assemblies modified by ion irradiation. *Nuclear Instruments and Methods in Physics Research Section B: Beam Interactions with Materials and Atoms*, 178(1–4):62–68, May 2001.

[TR95] H. Trinkaus and A. I. Ryazanov. Viscoelastic Model for the Plastic Flow of Amorphous Solids under Energetic Ion Bombardment. *Physical Review Letters*, 74(25):5072–5075, June 1995.

[UBNM15] Herbert M. Urbassek, R. Mark Bradley, Maureen L. Nietiadi, and Wolfhard Möller. Sputter yield of curved surfaces. *Physical Review B*, 91(16):165418, April 2015.

[vDSF+01] T van Dillen, E Snoeks, W Fukarek, C. M van Kats, K. P Velikov, A van Blaaderen, and A Polman. Anisotropic deformation of colloidal particles under MeV ion irradiation. *Nuclear Instruments and Methods in Physics Research Section B: Beam Interactions with Materials and Atoms*, 175–177:350–356, April 2001.

[Vol91] C. A. Volkert. Stress and plastic flow in silicon during amorphization by ion bombardment. *Journal of Applied Physics*, 70(7):3521–3527, October 1991.

[VWMS08] C. Verdeil, T. Wirtz, H. N. Migeon, and H. Scherrer. Angular distribution of sputtered matter under Cs+ bombardment with oblique incidence. *Applied Surface Science*, 255(4):870–873, December 2008.

[WKW04] W. Wesch, A. Kamarou, and E. Wendler. Effect of high electronic energy deposition in semiconductors. *Nuclear Instruments & Methods in Physics Research Section B-Beam Interactions with Materials and Atoms*, 225(1-2):111–128, August 2004. WOS:000223792600010.

[WM08] T. Wirtz and H. N. Migeon. Storing Matter: A new quantitative and sensitive analytical technique. *Applied Surface Science*, 255(4):1498–1500, December 2008.

[ZS95] Vladimir I. Zaporozchenko and Maria G. Stepanova. Preferential sputtering in binary targets. *Progress in Surface Science*, 49(2):155–196, June 1995.